*Conference Proceedings of the 5th Asia Pacific Luminescence and Electron Spin Resonance Dating Conference
October 15th-17th, 2018, Beijing, China*

Guest Editor: Grzegorz Adamiec

COMPARISON OF EQUIVALENT DOSES OBTAINED WITH VARIOUS post-IR IRSL DATING PROTOCOLS OF K-FELDSPAR

**JUNJIE ZHANG[1], SHENG-HUA LI[1], XULONG WANG[2], QINGZHEN HAO[3, 4, 5],
GUIMING HU[1] and YIWEI CHEN[6]**

[1]*Department of Earth Sciences, The University of Hong Kong, Hong Kong, China*
[2]*State Key Laboratory of Loess and Quaternary Geology, Institute of Earth Environment, Chinese Academy of Sciences,
Xi'an 710061, China*
[3]*Key Laboratory of Cenozoic Geology and Environment, Institute of Geology and Geophysics, Chinese Academy of Sciences,
Beijing 100029, China*
[4]*University of Chinese Academy of Sciences, Beijing 100049, China*
[5]*CAS Center for Excellence in Life and Paleoenvironment, Beijing, 100044, China*
[6]*State Key Laboratory of Isotope Geochemistry, Guangzhou Institute of Geochemistry, Chinese Academy of Sciences,
Guangzhou 510640, China*

Abstract: Five dating protocols with post-infrared infrared (IR) stimulated luminescence signals (*i.e.* pIRIR) were performed on the K-feldspar of loess samples. Two of them were the single-aliquot regenerative-dose protocol (SAR) with two-step pIRIR stimulation, with the first IR stimulation at 50°C or 200°C and the second at 290°C (pIR$_{50}$IR$_{290}$, pIR$_{200}$IR$_{290}$). Two of them were the SAR protocols with five-step or six-step IR stimulation at multiple elevated temperatures to 250°C or 300°C (MET-pIRIR$_{250}$, MET-pIRIR$_{300}$). The final one was the multiple-aliquot regenerative-dose (MAR) protocol with the MET-pIRIR$_{300}$ signal, together with a 500°C heat treatment administered before the test dose ('MAR with heat'). The results show that when the equivalent dose (D_e) of the sample was less than 500 Gy, all of the protocols gave consistent results; however, when D_e exceeded 750 Gy, all of the SAR protocols underestimated D_e. The pIR$_{50}$IR$_{290}$ signal had the highest degree of underestimation, while the pIR$_{200}$IR$_{290}$, MET-pIRIR$_{250}$ and MET-pIRIR$_{300}$ signals had similar D_e values and similar degrees of underestimation. Possible reasons for the SAR D_e underestimation are discussed. We suggest that only the 'MAR with heat' protocol is suitable for samples with D_e exceeding 750 Gy.

Keywords: Chinese loess, Potassium feldspar, pIRIR protocols, age underestimations.

Corresponding author: S.-H. Li
e-mail: shli@hku.hk

1. INTRODUCTION

Optically stimulated luminescence (OSL) dating is used to measure the period from the present to a mineral's last exposure to sunlight (Aitken, 1998). In order to obtain an OSL age, the equivalent dose (D_e) that minerals received after burial, together with the dose rate, need to be measured. The two minerals most commonly used for OSL dating are quartz and K-feldspar. Compared with quartz, the infra-red stimulated luminescence (IRSL) signal of K-feldspar has several advantages, such as high signal intensity, high internal dose rate, late saturation and uniform behaviour (e.g. Duller, 1997; Huntley and Lamothe, 2001; Li et al., 2007). However, OSL dating with K-feldspar has been hampered by the anomalous fading behaviour of the IRSL signal (e.g. Wintle, 1973; Spooner, 1992; 1994).

Notably, it was reported that the IRSL signal stimulated at a high-temperature following a preceding low-temperature IR stimulation was much more stable (Thomsen et al., 2008; 2011; Li and Li, 2011a). A two-step post-IR IRSL (pIRIR) dating protocol was proposed with the first stimulation at 50°C and the second stimulation at 225°C or 290°C (e.g. Buylaert et al., 2009; Thiel et al., 2011). However, subsequent studies indicated that the $pIR_{50}IR_{290}$ signal would still underestimate the age when D_e exceeded 500 Gy, since a small degree of fading still exists for this signal (Li and Li, 2012a; Li et al., 2014; Stevens et al., 2018). Consequently, the first stimulation temperature was increased to 200°C for the dating of relatively old samples (e.g. Li and Li, 2012a; Buylaert et al., 2015; Stevens et al., 2018).

A multiple-elevated-temperature post-IR IRSL (MET-pIRIR) dating protocol has been established with five or six steps of IR stimulation from 50°C to 250°C or 300°C, with an interval of 50°C (Li and Li, 2011b; 2012b). The anomalous fading test indicated that the fading rates of the MET-pIRIR signals at 250°C or 300°C were negligible (Li and Li, 2011b; 2012b). In order to extend the maximum dating limit, a protocol was proposed based on the dose-dependent sensitivity of MET-pIRIR signals using the multiple-aliquot regenerative-dose (MAR) protocol (Li et al., 2013; Chen et al., 2015). In this protocol, two repeated test doses were added after the regenerative dose, with a 'cut-heat to 500°C' treatment administered before the second test dose. With this protocol, the maximum dating limit of D_e was increased to ~1500 Gy (Li et al., 2013; Chen et al., 2015). Here, we use the term 'MAR with heat' to represent this protocol.

In the present study, K-feldspar samples from the Jingbian site on the northern margin of the Chinese Loess Plateau were dated using five pIRIR protocols: four SAR ($pIR_{50}IR_{290}$, $pIR_{200}IR_{290}$, MET-pIRIR$_{250}$, MET-pIRIR$_{300}$) protocols, and the 'MAR with heat' protocol. Subsequently, the D_e values obtained with the five protocols were compared.

2. SAMPLES AND MEASUREMENTS

Sample description

Samples were collected from two loess sections (A and B) at the Jingbian loess site, which is located on the northern margin of the Chinese Loess Plateau, adjacent to the Mu Us Desert (**Fig. 1a**). Paleoclimatic reconstructions and OSL dating have previously been conducted at the site (e.g. Ding et al., 2005; Buylaert et al., 2015; Stevens et al., 2018). Fine sand grains in this section are relatively abundant, ensuring sufficient coarse K-feldspar grains for the measurements. The well-bleached nature of loess samples makes them well suited for testing dating protocols. The samples were collected using stainless
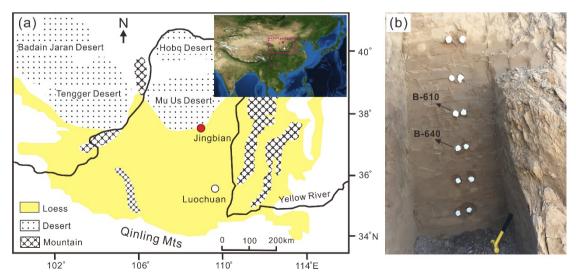

Fig. 1. a) Locations of the Jingbian and Luochuan loess sections. b) Photograph of the sampling of section B at Jingbian.

steel tubes to avoid light exposure (**Fig. 1b**). In section A, two samples were collected from the S1 and S2 paleosol layers, respectively; and in section B, four samples were collected from the layer which was assumed to be S2 based on field observation (e.g. colour, moisture).

Sample preparation and measurements

Sample pretreatment was performed in a dark room under subdued red light. Sample material from the two ends of the tubes was removed, and then the inner part was wet sieved to separate the >63 μm fraction, which was then successively treated with 10% HCl and 30% H_2O_2 solutions to remove carbonates and organic matter, respectively. The samples were then rinsed several times with water, oven-dried at 50°C overnight, and then dry sieved. The 90–125 μm fraction was used to separate K-feldspar grains, using a sodium poly-tungstate solution (ρ <2.58 g/cm^3). K-feldspar grains were immersed in 10% HF solution, with magnetic stirring, for ~15min, in order to remove the outer layer exposed to alpha irradiation. According to Duval *et al.* (2018), this treatment is sufficient to remove the outer 10 μm of K-feldspar grains. Etched K-feldspar grains were then mounted on steel discs with silicone oil. The IRSL measurements were performed using a Risø-TL/OSL-20 reader, with a filter package comprising a Schott BG-39 and Corning 7–59. The attached $^{90}Sr/^{90}Y$ beta source had a dose rate of 0.14 Gy/s on the steel discs. The first 10 s of the decay curve was integrated as the signal, with the final 10 s integrated as background. Details of the protocols are listed in **Table 1**.

In addition, the low-frequency magnetic susceptibility (MS) of dried samples was measured using a Bartington Instruments MS2 meter. Measurements were repeated three times, and the mean values were normalised by the sample weights to obtain the mass-specific MS (10^{-8} m^3/kg).

D_e and dose rate estimations

Standard growth curves (SGCs) were constructed to save measurement time. SGC constructions for the SAR protocols applied the least-squares normalisation (LS-normalization) method implemented with the R package 'numOSL' (Li *et al.*, 2016; 2017a; 2018; Peng and Li, 2017). In order to obtain D_e with the SAR SGC, aliquots were measured using two cycles, with the first cycle measuring the sensitivity-corrected natural signal (L_n/T_n), and the second cycle measuring the sensitivity-corrected signal (L_x/T_x) of a regenerative dose. Details of the calculation of D_e have been presented previously (Li *et al.*, 2015a, 2015b; 2017a; Zhang and Li, 2019). As the size of the test dose affects the shapes of growth curves, test doses were fixed at 300 Gy for SGC construction and D_e measurements.

For the "MAR with heat" protocol, samples from both the Jingbian section and the Luochuan section were used to construct the MAR SGC. Test doses were fixed at 100 Gy. Aliquots were first bleached using the ORIEL solar simulator (Newport Corporation, model 94042A) with a 1000W xenon arc lamp for more than 8 hr. Experiments showed that the residual doses of the MET-pIRIR$_{300}$ signals are reduced to ~10 Gy after bleaching

Table 1. *The five post-IR IRSL dating protocols used in this study. The first four are the SAR protocols with pIR$_{50}$IR$_{290}$, pIR$_{200}$IR$_{290}$, MET-pIRIR$_{250}$ and MET-pIRIR$_{300}$ signals, respectively. The fifth is the MAR protocol with the MET-pIRIR$_{300}$ signal and a 'cutheat to 500°C' treatment added before the test dose, simplified as 'MAR with heat' (modified from Li et al. (2013)).*

Step	SAR pIR$_{50/200}$IR$_{290}$		SAR MET-pIRIR$_{250/300}$		'MAR with heat'	
	Treatment	Observed	Treatment	Observed	Treatment	Observed
1	**Regenerative dose, *Di***		**Regenerative dose, *Di***		**Regenerative dose, *Di***	
2	Preheat at 320°C, 60 s		Preheat at 300°C or 320°C, 60 s		Preheat at 320°C, 60 s	
3	IRSL 200 s at 50/200°C		IRSL 100 s at 50°C		IRSL 100 s at 50°C	
4	IRSL 200 s at 290°C	L_x (290)	IRSL 100 s at 100°C		IRSL 100 s at 100°C	
5			IRSL 100 s at 150°C		IRSL 100 s at 150°C	
6			IRSL 100 s at 200°C		IRSL 100 s at 200°C	
7			IRSL 100 s at 250°C	Lx (250)	IRSL 100 s at 250°C	
8			IRSL 100 s at 300°C or not	Lx (300)	IRSL 100 s at 300°C	Lx (300)
9					**Cutheat to 500°C**	
10	**Test dose, *Dt***		**Test dose, *Dt***		**Test dose, *Dt***	
11	Preheat at 320°C, 60 s		Preheat at 300°C or 320°C, 60 s		Preheat at 320°C, 60 s	
12	IRSL 200 s at 50/200°C		IRSL 100 s at 50°C		IRSL 100 s at 50°C	
13	IRSL 200 s at 290°C	T_x (290)	IRSL 100 s at 100°C		IRSL 100 s at 100°C	
14	IR at 325°C, 200 s		IRSL 100 s at 150°C		IRSL 100 s at 150°C	
15	Return to step 1		IRSL 100 s at 200°C		IRSL 100 s at 200°C	
16			IRSL 100 s at 250°C	Tx (250)	IRSL 100 s at 250°C	
17			IRSL 100 s at 300°C or not	Tx (300)	IRSL 100 s at 300°C	Tx (300)
			IR at 320 or 325°C, 100 s			
			Return to step 1			

for 8 hr (**Fig. 2**). Bleached aliquots were divided into several groups, with different doses administered. For each sample, a group of aliquots was given a dose of 500 Gy. The average L_x/T_x of the aliquots with 500 Gy wa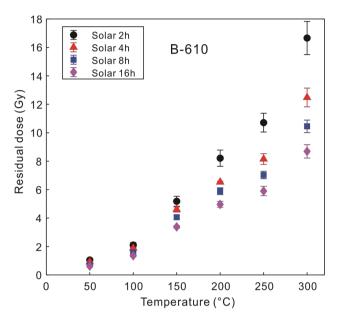s used to re-normalise the L_x/T_x values of all the aliquots for each sample, and the re-normalised L_x/T_x values were plotted against the doses and fitted with a single or double saturating exponential function (**Fig. 3**). The growth curve with the single saturating exponential function can be expressed as y = 0.100+1.755*(1–exp(–x/695)). In order to measure D_e with the MAR SGC, two groups of aliquots were prepared. One group of aliquots was used to measure the natural signal (L_n/T_n), and the other group of aliquots was bleached for more than 8 hr and then given a specific dose that was close to D_e, and the signals were measured (L_x/T_x). The average L_n/T_n of aliquots in the first group was normalised by the average L_x/T_x of aliquots in the second group, in order to calculate D_e. Outliers of the individual L_n/T_n or L_x/T_x values were identified and rejected by comparing the absolute deviation from the median value and the median absolute deviation using the criterion of 2.5 (Rousseeuw *et al.*, 2006; Hu *et al.*, 2019). The error in D_e was estimated using the error propagation formula.

Environmental dose rates were also estimated. Thick source alpha counting was performed to quantify the contribution of U and Th to the dose rate, and the K content of the whole rock was measured by X-ray fluorescence (XRF) analysis. Conversion factors were adopted from Adamiec and Aitken (1998). The internal K and Rb concentrations of the K-feldspar were assumed to be 13 ± 1% and 400 ± 100 ppm, respectively (Huntley and Baril, 1997; Zhao and Li, 2005). The dose rate of cosmic rays was calculated according to the sampling altitude, depth, and geomagnetic latitude (Prescott and Hutton, 1994). For the Jingbian section, the water content was generally set as 15 ± 5% for samples in paleosol layers,

Fig. 2. *Residual doses of IRSL signals stimulated at different temperatures using the SAR MET-pIRIR protocol. After 8 hr of bleaching with the solar simulator, the residual doses were reduced to ~10 Gy for the MET-pIRIR300 signal.*
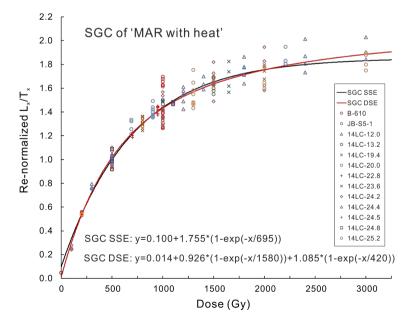

Fig. 3. *Standard growth curve (SGC) of the 'MAR with heat' protocol. The re-normalisation dose was 500 Gy. SGC curves were fitted with the single saturating exponential (SSE) function: y = y0 + A*(1-exp(-x/D0)) and the double saturating exponential (DSE) function: y = y0 + A1*(1-exp(-x/D1)) + A2*(1-exp(-x/D2)), respectively. The fitted results are shown in the graph. Note that the two SGCs only begin to diverge when the dose exceeds 2000 Gy.*

and 10 ± 5% for samples in loess layers (Stevens *et al.*, 2018). However, for sample B-610, where an MS peak was located, the water content was measured to be 19.3% for sample material from the inner part of the sampling tube, and we adopted the measured water content for dose rate calculation. Because of the close similarity of depths and MS values between samples B-610 and B-640, we assumed that sample B-640 also had a water content of 19.3 ± 5%.

3. RESULTS

The D_e values of the two sections are listed in **Table 2**, and the dose rates and corresponding ages are listed in **Table 3**. The residual doses are not considered as they are negligible compared to the D_e values (**Fig. 2**). In section A, for the sample from paleosol S1 (A-570), the D_e values are consistent (~400 Gy) between the protocols. However, for the sample from paleosol S2 (A-1050), with the SAR protocol, the D_e values are ~620 Gy for the $pIR_{50}IR_{290}$ signal and ~700 Gy for the $pIR_{200}IR_{290}$ and MET-pIRIR$_{250}$ signals. With the 'MAR with heat' protocol, D_e increased to ~750 Gy.

In section B, the D_e values and ages of samples are plotted against depth in **Fig. 4**. The D_e values are overall greater than 500 Gy. With the SAR protocol, the $pIR_{50}IR_{290}$ signal always gave the smallest D_e values (540–650 Gy), while the $pIR_{200}IR_{290}$, MET-pIRIR$_{300}$ signals generally had consistent D_e values (640–820 Gy). However, all of the SAR D_e values are smaller than those of the 'MAR with heat' protocol with the MET-pIRIR$_{300}$ signal (860–930 Gy). The ages of the

four samples are 160–190 ka for the $pIR_{50}IR_{290}$ signal, and 190–240 ka for the $pIR_{200}IR_{290}$, MET-pIRIR$_{250}$, MET-pIRIR$_{300}$ signals with the SAR protocol. With the 'MAR with heat' protocol, the ages are 250–260 ka (excluding the error).

4. DISCUSSION

Possible cause of D_e underestimation with the SAR protocol

It was reported that the $pIR_{50}IR_{290}$ signal was not applicable for dating samples with D_e values exceeding 500 Gy, because the effect of anomalous fading cannot be adequately removed; whereas the $pIR_{200}IR_{290}$ and MET-pIRIR$_{250}$ signals were sufficiently stable to date older samples (Li and Li, 2012a). Here, we found that the $pIR_{200}IR_{290}$ and MET-pIRIR$_{250}$ or MET-pIRIR$_{300}$ signals also failed in dating samples with D_e exceeding ~750 Gy, as long as the SAR protocol was used. With the identical signal, the 'MAR with heat' protocol always had a larger D_e than the SAR protocol (**Fig. 5**). Therefore, the failure of the $pIR_{200}IR_{290}$, MET-pIRIR$_{250}$, MET-pIRIR$_{300}$ signals with the SAR protocol for D_e estimation was not related to the signal stability but rather related to the SAR protocol itself.

Previous studies have shown that the pattern of sensitivity changes of K-feldspar in the first cycle of the SAR protocol may be dissimilar to the pattern of sensitivity change in the subsequent cycles and that the failure of sensitivity correction of the first cycle would result in the underestimation of D_e for low-temperature IRSL signals (Wallinga *et al.*, 2000; Chen *et al.*, 2013; Kars *et al.*,

Table 2. D_e values obtained using the five protocols. In the 'MAR with heat' protocol, the first 'n' indicates the aliquots used to measure the natural signal, and the second refers to the aliquots used to measure the signal of a regenerative dose.

Sample	Depth (cm)	SAR pIR$_{50}$IR$_{290}$ D_e ± σ	n	SAR pIR$_{200}$IR$_{290}$ D_e ± σ	n	SAR MET-pIRIR$_{250}$ D_e ± σ	n	SAR MET-pIRIR$_{300}$ D_e ± σ	n	MAR with heat D_e ± σ	n
A-570	570	373 ± 35	7	424 ± 11	19	415 ± 9	15	\	\	381 ± 11	12;12
A-1050	1050	615 ± 54	7	706 ± 34	8	706 ± 17	8	\	\	747 ± 53	16;8
B-0	220	543 ± 17	6	673 ± 57	4	640 ± 13	8	712 ± 57	6	856 ± 73	24;14
B-610	830	652 ± 20	10	734 ± 21	14	753 ± 17	9	773 ± 45	6	925 ± 62	24;20
B-640	860	613 ± 51	6	741 ± 18	9	773 ± 22	7	749 ± 57	6	901 ± 51	14;10
B-1000	1190	649 ± 61	6	822 ± 35	5	762 ± 25	7	800 ± 47	6	897 ± 71	24;20

Table 3. Dose rates and ages of the samples using the five protocols.

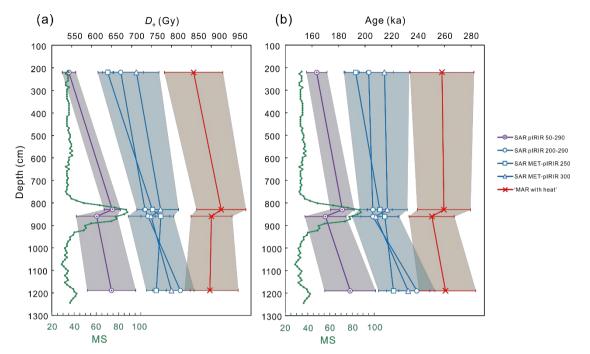| Sample	Water (%)	K$_2$0 (%)	Alpha count	Dose rate (Gy/ka)	Age (ka) SAR pIR$_{50}$IR$_{290}$	SAR pIR$_{200}$IR$_{290}$	SAR MET-pIRIR$_{250}$	SAR MET-pIRIR$_{300}$	MAR with heat
A-570	15 ± 5	2.03	9.55 ± 0.15	3.21 ± 0.12	116 ± 12	132 ± 6	129 ± 6	\	119 ± 6
A-1050	15 ± 5	2.19	10.83 ± 0.16	3.44 ± 0.13	179 ± 17	206 ± 13	206 ± 9	\	217 ± 17
B-0	15 ± 5	1.95	10.14 ± 0.18	3.30 ± 0.12	165 ± 8	204 ± 19	194 ± 8	216 ± 19	260 ± 24
B-610	19.3 ± 5	2.50	11.88 ± 0.19	3.55 ± 0.13	183 ± 9	206 ± 10	212 ± 9	217 ± 15	260 ± 20
B-640	19.3 ± 5	2.40	11.85 ± 0.19	3.59 ± 0.13	171 ± 16	206 ± 9	215 ± 10	209 ± 18	251 ± 17
B-1000	15 ± 5	2.22	10.74 ± 0.18	3.43 ± 0.13	189 ± 19	240 ± 14	222 ± 11	233 ± 16	261 ± 23

Fig. 4. D_e values and age versus depth relationship for section B. The SAR pIR$_{50}$IR$_{290}$ protocol has the youngest ages; the SAR pIR$_{50}$IR$_{290}$, MET-pIRIR$_{250}$ and MET-pIRIR$_{300}$ protocols have similar ages; and the 'MAR with heat' protocol has the oldest ages.

2014; Li *et al.*, 2017a; Qin *et al.*, 2018; Zhang, 2018). The difference between the patterns of sensitivity change in the first and subsequent cycles was initially attributed to the increase in the electron trapping probability caused by the first preheat treatment (Wallinga *et al.*, 2000; Kars *et al.*, 2014; Zhang, 2018). However, a later study found that it was due to the combination of the decrease in the electron trapping probability and the increase in recombination probability (Qin *et al.*, 2018). For low-temperature IRSL signals, such as IR$_{50}$, the failure of sensitivity correction would always result in D_e underestimation when the preheat temperature was high (e.g. 200°C) (Wallinga *et al.*, 2000; Kars *et al.*, 2014; Zhang, 2018). However, for high-temperature pIRIR signals, the sensitivity correction of the first cycle is generally acceptable (Kars *et al.*, 2014; Li *et al.*, 2017a; Zhang, 2018), and dose recovery ratios are close to unity (Kars *et al.*, 2014; Zhang, 2018). Nevertheless, a slight underestimation or overestimation of dose recovery ratios can occur, depending on the type of pIRIR signal, the magnitude of the regenerative dose and test dose, the preheat temperature (Qin *et al.*, 2018), as well as the sample origin (Zhang, 2018). In order to study the influence, sample B-1000 was used to perform the dose-recovery-like experiments which were the same as those used by Qin *et al.* (2018). The ORIEL solar simulator bleached about 15 aliquots for 20 hours and then divided into five groups, each group comprising ~3 aliquots. The given doses for the five groups were

0, 150, 300, 600, 900 Gy, respectively. The test dose was 300 Gy, the same as that used in the SAR D_e measurements. Two repeating cycles were carried out for each group with identical dose. The sensitivity-corrected MET-pIRIR$_{250}$ signal of the first cycle (L_1/T_1) can be treated as the natural signal, and that of the second cycle (L_2/T_2) can be treated as the regenerative dose signal. Growth curves of the two kinds of signals were constructed with all of the aliquots from the five groups (**Fig. 6a**). The growth curve of L_2/T_2 was in fact constructed using multiple aliquots, but it was equivalent to the laboratory growth curve of a single aliquot in the SAR protocol, because of the consistency between different aliquots and the excellent recycling ratios (near unity) in SAR cycles for K-feldspar. In order to calculate the recovery ratios, the given doses of the first cycle were taken as unknown, and the corresponding 'D_e' values were calculated based on the growth curve of L_2/T_2, using the gSGC method (Li *et al.*, 2015a, 2015b; Zhang and Li, 2019). The mean recovery ratio was calculated for each group and plotted against the recovery dose (**Fig. 6b**). The results show that with the test dose of 300 Gy, the recovery ratio became slightly overestimated when the recovery dose exceeded 600 Gy. Therefore, the failure of the sensitivity correction of the first cycle in the SAR protocol cannot explain the SAR D_e underestimation observed in this study.
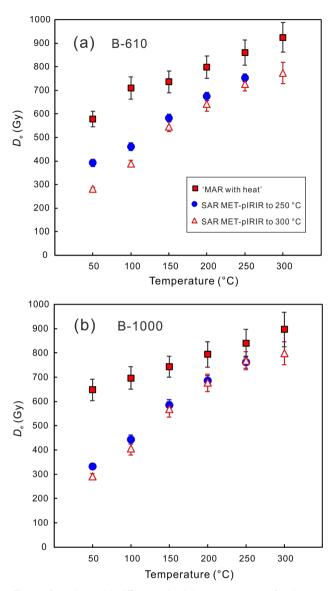
Fig. 5. *D_e values with different stimulation temperatures for the two SAR protocols with MET-pIRIR stimulation to 250°C or 300°C, and the 'MAR with heat' protocol. Note that the MAR D_e values always exceed the SAR De values.*
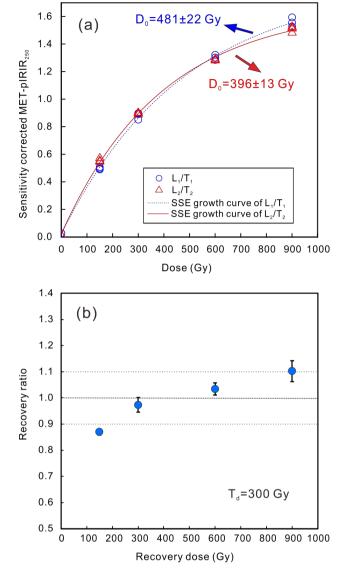
Fig. 6. *Results of dose-recovery-like experiments for sample B-1000. (a) The growth curves of the L_1/T_1 and L_2/T_2 signals fitted with a single saturating exponential (SSE) function: $y = y_0 + a*(1-exp(-x/D_0))$. (b) Regenerative doses of the first cycle are taken as unknown and recovered by the growth curve of L_2/T_2. The recovery ratios are plotted versus the recovery doses. Note that the recovery ratios are slightly overestimated when the doses exceed 600 Gy.*

With the SAR protocol, the growth curve of K-feldspar has D_0 of ~ 400 Gy (**Fig. 6a**). The beginning point of SAR D_e underestimation is ~750 Gy, which is very close to $2D_0$. For quartz, it has been proposed that reliable D_e estimation should be within the upper limit of $2D_0$ (Wintle and Murray, 2006). Age underestimation has been observed when applying quartz OSL dating in marine isotope stage 5, with D_e values close to the $2D_0$ limit (e.g. Murray and Funder, 2003; Lai, 2010). It appears that the empirical $2D_0$ limit also exists for K-feldspar. A recent study suggested that D_e underestimation for quartz when exceeding the $2D_0$ limit, was caused by the rejection of 'saturated' grains or aliquots, and an 'average

L_n/T_n' method was thus proposed to overcome the problem (Li *et al.*, 2017b). Successful application of this method has been performed on archeological cave sediments with an age range of 170–80 ka (Hu *et al.*, 2019). For the K-feldspar samples used in the present study, no 'saturated' aliquots were identified for the SAR protocols. With the application of the 'average L_n/T_n' method, D_e became slightly smaller than the values obtained using the conventional 'average D_e' method.

We can provide no credible hypothesis to explain the SAR D_e underestimation in the high dose range in the present study. It is possible that the natural growth curve and laboratory growth curve of K-feldspar begin to diverge in the high dose range, similar to the case for quartz (Timar-Gabor and Wintle, 2013). However, it cannot explain the different behaviour of the SAR protocol and the 'MAR with heat' protocol and therefore, further studies are needed in the future.

Implications for dating

As shown in **Fig. 3**, the growth curve of the 'MAR with heat' protocol saturates much later, with D_0 of ~700 Gy (Li *et al.*, 2013; Chen *et al.*, 2015). Application of the $2D_0$ limit would enable reliable dating to ~1400 Gy. In addition, with the MAR protocol, the discrepancy between the sensitivity changes between the first and subsequent cycles within the SAR protocol is not a concern, since all the aliquots were run for only one cycle. The '500°C heat' inserted before the test dose was designed to erase pre-dose memory (Li *et al.*, 2013; Chen *et al.*, 2015). Although a large sensitivity change would also result from such a high-temperature treatment, it would not influence the reliability of D_e measurements, as the signal of the subsequent test dose is now solely related to the size of the aliquots. The test dose signal is used for mass normalisation between different aliquots, rather than sensitivity correction. Thus, for old samples, the D_e values obtained with the 'MAR with heat' protocol are the most accurate.

The SAR ages of the four samples from section B range from 160–190 ka with the $pIR_{50}IR_{290}$ signal, and 190–240 ka with the $pIR_{200}IR_{290}$, MET-$pIRIR_{250}$, MET-$pIRIR_{300}$ signals, which correspond to loess layer L2 and paleosol layer S2, respectively. The ages obtained using the 'MAR with heat' protocol are systematically 30–40 ka older than the SAR ages with the same MET-$pIRIR_{300}$ signal. Considering the errors of ~20 ka for the MAR ages, it is uncertain whether the samples are located in S2 layer or L3 layer.

5. CONCLUSIONS

By comparing D_e measurements on K-feldspar using five post-IR IRSL dating protocols, we found that D_e values did not change substantially between different protocols when the D_e values were less than 500 Gy. However, when the D_e values exceeded 750 Gy, the SAR dating protocols with $pIR_{50}IR_{290}$, $pIR_{200}IR_{290}$, MET-$pIRIR_{250}$ or MET-$pIRIR_{300}$ signals underestimated D_e; in addition, the $pIR_{50}IR_{290}$ signal had a higher degree of underestimation due to the signal instability. However, for the $pIR_{200}IR_{290}$, MET-$pIRIR_{250}$, MET-$pIRIR_{300}$ signals, the D_e underestimation was not due to the signal instability, and neither was it due to the failure of sensitivity correction of the first cycle in the SAR protocol. No reasonable explanation can be proposed here for the SAR D_e underestimation in the high dose range.

Compared to SAR protocols, the 'MAR with heat' protocol can provide the most reliable D_e estimation for old samples with D_e exceeding 750 Gy.

REFERENCES

Adamiec G and Aitken MJ, 1998. Dose-rate conversion factors: update. *Ancient TL* 16: 37–50.

Aitken MJ, 1998. An Introduction to Optical Dating. Oxford University Press, Oxford.

Buylaert JP, Yeo EY, Thiel C, Yi SW, Stevens T, Thompson W, Frechen M, Murray A and Lu HY, 2015. A detailed post-IR IRSL chronology for the last interglacial soil at the Jingbian loess site (northern China). *Quaternary Geochronology* 30: 194–199, DOI 10.1016/j.quageo.2015.02.022.

Buylaert JP, Murray AS, Thomsen KJ and Jain M, 2009. Testing the potential of an elevated temperature IRSL signal from K-feldspar. *Radiation Measurements* 44: 560–565, DOI 10.1016/j.radmeas.2009.02.007.

Chen YW, Li SH and Li B, 2013. Residual doses and sensitivity change of post IR IRSL signals from potassium feldspar under different bleaching conditions. *Geochronometria* 40: 229–238, DOI 10.2478/s13386-013-0128-3.

Chen YW, Li SH, Li B, Hao QZ and Sun JM, 2015. Maximum age limitation in luminescence dating of Chinese loess using the multiple-aliquot MET-pIRIR signals from K-feldspar. *Quaternary Geochronology* 30: 207–212, DOI 10.1016/j.quageo.2015.01.002.

Ding ZL, Derbyshire E, Yang SL, Sun JM and Liu TS, 2005. Stepwise expansion of desert environment across northern China in the past 3.5 Ma and implications for monsoon evolution. *Earth and Planetary Science Letters* 237: 45–55, DOI 10.1016/j.epsl.2005.06.036.

Duller GAT, 1997. Behavioural studies of stimulated luminescence from feldspars. *Radiation Measurements* 27: 663–694, DOI 10.1016/S1350-4487(97)00216-3.

Duval M, Guilarte V, Campaña I, Arnold LJ, Miguens L, Iglesias J and González-Sierra S, 2018. Quantifying hydrofluoric acid etching of quartz and feldspar coarse grains based on weight loss estimates: implication for ESR and luminescence dating studies. *Ancient TL* 36(1): 1–14.

Hu Y, Marwick B, Zhang J-F, Rui X, Hou Y-M, Yue J-P, Chen W-R, Huang W-W and Li B, 2019. Late Middle Pleistocene Levallois stone-tool technology in southwest China. *Nature* 565: 82–85, DOI 10.1038/s41586-018-0710-1.

Huntley DJ and Lamothe M, 2001. Ubiquity of anomalous fading in K-feldspars and the measurement and correction for it in optical dating. *Canadian Journal of Earth Sciences* 38: 1093–1106, DOI 10.1139/e01-013.

Huntley DJ and Baril MR, 1997. The K content of the K-feldspars being measured in optical dating or in thermoluminescence dating. *Ancient TL* 15: 11–13.

Kars RH, Reimann T and Wallinga J, 2014. Are feldspar SAR protocols appropriate for post-IR IRSL dating? *Quaternary Geochronology* 22: 126–136, DOI 10.1016/j.quageo.2014.04.001.

Lai ZP, 2010. Chronology and the upper dating limit for loess samples from Luochuan section in the Chinese Loess Plateau using quartz OSL SAR protocol. *Journal of Asian Earth Sciences* 37: 176–185, DOI 10.1016/j.jseaes.2009.08.003.

Li B, Jacobs Z and Roberts RG, 2016. Investigation of the applicability of standardised growth curves for OSL dating of quartz from Haua Fteah cave, Libya. *Quaternary Geochronology* 35: 1–15, DOI 10.1016/j.quageo.2016.05.001.

Li B, Jacobs Z and Roberts RG, 2017a. An improved multiple-aliquot regenerative-dose (MAR) procedure for post-IR IRSL dating of K-feldspar. *Ancient TL* 35(1): 1–10.

Li B, Jacobs Z, Roberts RG, Galbraith R and Peng J, 2017b. Variability in quartz OSL signals caused by measurement uncertainties: Problems and solutions. *Quaternary Geochronology* 41: 11–25, DOI 10.1016/j.quageo.2017.05.006.

Li B, Jacobs Z, Roberts RG and Li SH, 2013. Extending the age limit of luminescence dating using the dose-dependent sensitivity of MET-pIRIR signals from K-feldspar. *Quaternary Geochronology* 17: 55–67, DOI 10.1016/j.quageo.2013.02.003.

Li B, Jacobs Z, Roberts RG and Li SH, 2014. Review and assessment of the potential of post-IR IRSL dating methods to circumvent the problem of anomalous fading in feldspar luminescence. *Geochronometria* 41: 178–201, DOI 10.2478/s13386-013-0160-3.

Li B, Jacobs Z, Roberts RG and Li SH, 2018. Single-grain dating of potassium-rich feldspar grains: Towards a global standardised growth curve for the post-IR IRSL signal. *Quaternary Geochronology* 45: 23–36, DOI 10.1016/j.quageo.2018.02.001.

Li B and Li SH, 2011a. Thermal stability of infrared stimulated luminescence of sedimentary K-feldspar. *Radiation Measurements* 46: 29–36, DOI 10.1016/j.radmeas.2010.10.002.

Li B and Li SH, 2011b. Luminescence dating of K-feldspar from sediments: A protocol without anomalous fading correction. *Quaternary Geochronology* 6: 468–479, DOI 10.1016/j.quageo.2011.05.001.

Li B and Li SH, 2012a. A reply to the comments by Thomsen *et al.* on "Luminescence dating of K-feldspar from sediments: A protocol without anomalous fading correction". *Quaternary Geochronology* 8: 49–51, DOI 10.1016/j.quageo.2011.10.001.

Li B and Li SH, 2012b. Luminescence dating of Chinese loess beyond 130 ka using the non-fading signal from K-feldspar. *Quaternary Geochronology* 10: 24–31, DOI 10.1016/j.quageo.2011.12.005.

Li B, Roberts RG, Jacobs Z and Li SH, 2015a. Potential of establishing a 'global standardised growth curve' (gSGC) for optical dating of quartz from sediments. *Quaternary Geochronology* 27: 94–104, DOI 10.1016/j.quageo.2015.02.011.

Li B, Roberts RG, Jacobs Z, Li SH and Guo YJ, 2015b. Construction of a 'global standardised growth curve' (gSGC) for infrared stimulated luminescence dating of K-feldspar. *Quaternary Geochronology* 27: 119–130, DOI 10.1016/j.quageo.2015.02.010.

Li SH, Chen YY, Li B, Sun JM and Yang LR, 2007. OSL dating of sediments from deserts in northern China. *Quaternary Geochronology* 2: 23–28, DOI 10.1016/j.quageo.2006.05.034.

Murray AS and Funder S, 2003. Optically stimulated luminescence dating of a Danish Eemian coastal marine deposit: a test of accuracy. *Quaternary Science Reviews* 22: 1177–1183, DOI 10.1016/S0277-3791(03)00048-9.

Peng J and Li B, 2017. Single-aliquot Regenerative-Dose (SAR) and Standardised Growth Curve (SGC) Equivalent Dose Determination in a Batch Model Using the R Package 'numOSL'. *Ancient TL* 35(2): 32–53.

Prescott JR and Hutton JT, 1994. Cosmic-Ray Contributions to Dose-Rates for Luminescence and ESR Dating - Large Depths and Long-Term Time Variations. *Radiation Measurements* 23: 497–500, DOI 10.1016/1350-4487(94)90086-8.

Qin J, Chen J, Li Y and Zhou L, 2018. Initial sensitivity change of K-feldspar pIRIR signals due to uncompensated decrease in electron trapping probability: Evidence from radiofluorescence measurements. *Radiation Measurements* 120: 131–136, DOI 10.1016/j.radmeas.2018.06.017.

Rousseeuw PJ, Debruyne M, Engelen S and Hubert M, 2006. Robustness and outlier detection in chemometrics. *Critical Reviews in Analytical Chemistry* 36: 221–242, DOI 10.1080/10408340600969403.

Spooner NA, 1992. Optical Dating - Preliminary-Results on the Anomalous Fading of Luminescence from Feldspars. *Quaternary Science Reviews* 11: 139–145, DOI 10.1016/0277-3791(92)90055-D.

Spooner NA, 1994. The Anomalous Fading of Infrared-Stimulated Luminescence from Feldspars. *Radiation Measurements* 23: 625–632, DOI 10.1016/1350-4487(94)90111-2.

Stevens T, Buylaert JP, Thiel C, Ujvari G, Yi S, Murray AS, Frechen M and Lu H, 2018. Ice-volume-forced erosion of the Chinese Loess Plateau global Quaternary stratotype site. *Nature Communications* 9: 983, DOI 10.1038/s41467-018-03329-2.

Thiel C, Buylaert JP, Murray A, Terhorst B, Hofer I, Tsukamoto S and Frechen M, 2011. Luminescence dating of the Stratzing loess profile (Austria) - Testing the potential of an elevated temperature post-IR IRSL protocol. *Quaternary International* 234: 23–31, DOI 10.1016/j.quaint.2010.05.018.

Thomsen KJ, Murray AS and Jain M, 2011. Stability of IRSL Signals from Sedimentary K-Feldspar Samples. *Geochronometria* 38: 1–13, DOI 10.2478/s13386-011-0003-z.

Thomsen KJ, Murray AS, Jain M and Botter-Jensen L, 2008. Laboratory fading rates of various luminescence signals from feldspar-rich sediment extracts. *Radiation Measurements* 43: 1474–1486, DOI 10.1016/j.radmeas.2008.06.002.

Timar-Gabor A and Wintle AG, 2013. On natural and laboratory generated dose response curves for quartz of different grain sizes from Romanian loess. *Quaternary Geochronology* 18: 34–40, DOI 10.1016/j.quageo.2013.08.001.

Wallinga J, Murray A and Duller G, 2000. Underestimation of equivalent dose in single-aliquot optical dating of feldspars caused by preheating. *Radiation Measurements* 32: 691–695, DOI 10.1016/S1350-4487(00)00127-X.

Wintle AG, 1973. Anomalous Fading of Thermoluminescence in Mineral Samples. *Nature* 245: 143–144, DOI 10.1038/245143a0.

Wintle AG and Murray AS, 2006. A review of quartz optically stimulated luminescence characteristics and their relevance in single-aliquot regeneration dating protocols. *Radiation Measurements* 41: 369–391, DOI 10.1016/j.radmeas.2005.11.001.

Zhang JJ, 2018. Behavior of the electron trapping probability change in IRSL dating of K-feldspar: A dose recovery study. *Quaternary Geochronology* 44: 38–46, DOI 10.1016/j.quageo.2017.12.001.

Zhang JJ and Li SH, 2019. Constructions of standardised growth curves (SGCs) for IRSL signals from K-feldspar, plagioclase and poly-mineral fractions. *Quaternary Geochronology* 49: 8–15, DOI 10.1016/j.quageo.2018.05.015.

Zhao H and Li SH, 2005. Internal dose rate to K-feldspar grains from radioactive elements other than potassium. *Radiation Measurements* 40: 84–93, DOI 10.1016/j.radmeas.2004.11.004.